Spring 5-2002

Endotension Distribution in Finite Element Models of Abdominal Aortic Aneurysm Following Endovascular Exclusion

William Joseph Jenkins
University of Tennessee - Knoxville

Appendix D - UNIVERSITY HONORS PROGRAM SENIOR PROJECT - APPROVAL

Name: William J. Jenkins

College: Engineering Department: Mech., Aero., and Bio. Engr.

Faculty Mentor: Kara L. Kruse, Oak Ridge National Laboratory

PROJECT TITLE: Endotension Distribution in Finite Element Models of Abdominal Aortic Aneurysm Following Endovascular Exclusion

I have reviewed this completed senior honors thesis with this student and certify that it is a project commensurate with honors level undergraduate research in this field.

Signed: Kara L. Kruse, Faculty Mentor

Date: May 6' 2002

Comments (Optional):

May 6, 2002

Dr. Broadhead,

Bill did an excellent job on his honors project. Last summer he was in the Energy Research Undergraduate Laboratory Fellowship program at ORNL under my supervision. During this time, Bill worked on an idealized mode of the Abdominal Aortic Aneurysm (AAA). During the fall and spring semesters, Bill continued with the project and worked with Dr. John Pacanowski, M.D., a research Vascular Fellow at UTMCK, to develop numerical models of Dr. Pacanowski's physical experiments of endotension in synthetically created canine AAAs. Bill also attended weekly research meetings with the UTMCK Vascular Surgery team overseeing the research. Recently, Bill gave an impromptu demonstration of his work to visiting biomedical engineer Dr. Richard Komistek, President and Executive Director, of the Rocky Mountain Musculoskeletal Research Lab. Dr. Komistek was very impressed and commented that Bill's work was what he would have expected from a M.S.E. student rather than an undergraduate.

Sincerely,

Kara L. Kruse

Kara L. Kruse

Endotension Distribution in Finite Element Models of Abdominal Aortic Aneurysm Following Endovascular Exclusion

William J. Jenkins

Oak Ridge National Laboratory, Oak Ridge, Tennessee, USA
The University of Tennessee Medical Center, Knoxville, Tennessee, USA

Completed for the University of Tennessee Honors Program Senior Project under the supervision of Kara L. Kruse, M.S.E.

Correspondence: Kara L. Kruse, M.S.E. Division of Computational Sciences & Engineering, Oak Ridge National Laboratory, P.O. Box 2008 MS6418, Oak Ridge, TN 37831-6418, krusekl@ornl.gov, (865) 574-5154.

Abstract

Purpose: Endotension has been implicated in complications following the endovascular repair of abdominal aortic aneurysm (AAA) such as continued AAA expansion and rupture, proximal aneurysm neck dilation, and endovascular graft migration. To begin to evaluate the role of endotension in the mechanisms of post-repair problems, the magnitude and distribution of endotension in an excluded aneurysm must be understood. The purpose of this study is to determine how endotension is distributed throughout excluded aneurysms without endoleak.
Methods: Computational models of AAA were constructed using CT data of three experimental AAA models created from canine aortic tissue. Finite element analysis was used to simulate blood pressure loading and compute the resulting mechanical stress throughout the aneurysm. The computed stress patterns were used to evaluate how endotension is distributed throughout the aneurysm. Comparison of results between the computational and experimental models was made possible through simulating the experimental models with the computational models.
Results: Peak arterial wall stresses occurred at the ends of the aneurysm where the wall was in close proximity to the endograft. Conversely, the lowest wall stresses were computed at the bulge of the aneurysm where the wall was farthest from the graft. Peak aneurysm sac (AS) stresses were higher near the endograft than at the wall. The lowest AS stresses occurred near the wall at the bulge of the aneurysm. Peak endograft stresses occurred at regions on the graft corresponding to the bulge of the aneurysm where the wall was farthest away. The lowest endograft stresses were computed at the ends of the endograft where the wall and graft were in close proximity.
Conclusions: Endotension is a real phenomenon that occurs in absence of endoleak. Endotension in the aneurysm sac and wall is not uniformly distributed and attenuates with distance from the endograft. Conversely, endotension in the endograft is lowest where the wall is in close proximity. These results and conclusions complemented those of the experimental study of endotension.

Introduction

Commonly, AAAs are treated with minimally invasive endovascular repair to prevent rupture. The procedure involves implanting a stented vascular graft at the location of the aneurysm via catheterization from the femoral arteries. The purpose of the endovascular graft is to exclude the aneurysm sas (AS) from circulation resulting in the reduction of the pressure load on the aneurysm wall. By reducing the pressure load, the tension in the wall is reduced. However, despite endovascular repair, rupture remains a concern. One study showed that the majority of post-operative AAAs either had no change in diameter or an increase in diameter within three months or more.[1] It is the reduction in diameter of an AAA that is thought to indicate the reduction of tension[2] and, in turn, the stress in the wall. In either case, the potential for rupture remains.

One factor that has been implicated in post-repair aneurysm expansion and rupture is endotension, the persistent pressurization of an aneurysm sac despite endovascular exclusion. Correlations between endotension without endoleak and continued AAA expansion and rupture[3,4,5], proximal aneurysm neck dilation[3,6], and endograft migration[7] have been proposed. However, little is understood about the magnitude of endotension or how endotension is distributed throughout the excluded aneurysm. Before the relationships between endotension and mechanisms of continued AAA expansion, neck dilation, and endograft migration can be understood, the magnitude and distribution of endotension in post-repair AAAs must be characterized.

To determine the distribution of endotension without endoleak, a combined study was performed using both experimental and computational models of post-endovascular AAA repair. In the experimental models, artificial aneurysms were created from canine aortic tissue, subjected to blood flow, placed on a pulsatile pump system, and excluded with an endovascular graft.[8] Endotension distribution was studied by measuring pressure with a strain gauge in the aneurysm sac at various locations with several different consistencies of the AS contents such as unclotted blood, fresh thrombus, and fibrin thrombus.

The experimental models were reconstructed on computer using CT images. Endotension distribution was studied by using the finite element (FE) method to simulate blood pressure loading and compute the resulting mechanical stress throughout the aneurysm. The stress patterns found in the aneurysm were used to evaluate how endotension is distributed. An assumption of this study is that endotension can be described by mechanical stress.

The experimental and computational studies were designed to allow comparison of their results and conclusions. The purpose of combining these experiments is to utilize the advantages of both of their methods. The experimental aneurysms are a more realistic model of human AAAs having biologic tissues, an endovascular graft, pulsatile blood flow, etc. However, endotension can be measured only at a few specific points in the aneurysm sac. Further, the manner in which endotension is transmitted to the wall cannot be directly described from AS measurements. Conversely, the finite element method computes mechanical stress at all locations in the model (wall, AS, and endograft). Thus, the entire picture of endotension throughout the aneurysm is seen. However, there are many simplifications to the experimental models, such as static pressure loading and linear tissue elasticity, that are made to create FE models that can be

analyzed and have obtainable solutions. Thus, the computational models provide more information on the distribution of endotension, but a higher confidence in the results is attained for the experimental models because of its fewer number of simplifications. The results and conclusions of the experimental model have been published[8], and this article reports the findings of the computational study.

Method

Finite element (FE) models of AAA were generated from CT scans of three artificial aneurysms created from canine aortic tissue in the associated experimental study.[8] These artificial aneurysms were studied after excluding the aneurysm sac (AS) with an endovascular graft, allowing the blood in the AS to thrombose, and subjecting the model to a pulsatile blood flow system. The first step in creating the FE models was to define the luminal and wall boundaries in each CT image using commercially available image segmentation software (SURFdriver 3.5, Moody & Lozanoff). Lumen and wall contours initially were defined by a series of points every 3-5 mm along the lumen or wall boundary in a CT image. Wall contours were defined for every three to four images resulting in an axial resolution of 3-4 mm. Further, 3-4 mm separated the images containing the wall contours. Because of the simpler geometry of the endograft, lumen contours were defined every five to seven images with a corresponding axial resolution of 5-7 mm.

The points defining the wall and lumen contours were imported into another software package (MSC.Patran 2001), and a 4-parameter, uniform Bspline smoothing algorithm was used to create new curves defining the wall and lumen contours that were continuous on the first and second derivatives. Next, AAA wall and lumen surfaces were generated from an algorithm that interpolated between the contours in the axial direction. This algorithm maintained the second order continuity of the AAA surface geometry, a property shown to be important in this type of AAA finite element analysis.[9] The 3-D solid representing the AS contents was defined using the wall and lumen surfaces, which make up its bounding surfaces.

Having recreated the geometry of the artificial AAA, the material properties of the wall, endograft, and AS contents were defined. All three materials were assumed to be linearly elastic, homogenous, incompressible, and isotropic. Because the elastic properties of canine and human aortic tissue are similar, an experimentally determined value for the elastic modulus of human aortic tissue, 5 MPa[10,11], was used to define the elasticity of the wall. An experimentally determined value for organized intraluminal thrombus, 0.2 MPa[12], was used to define the elastic modulus for the AS contents (assumed to be thrombosed). Properties for the stent-graft were not readily available. An approximate value of 5 MPa for the elastic modulus was used, which is similar to the stiffness of abdominal aortic wall tissue and of polytetraflouroethylene (PTFE) vascular grafts.[13] The other material property definition used for the wall, endograft, and AS contents was Poisson's ratio. Instead of using 0.5 for Poisson's ratio for complete incompressibility, 0.49 was used to decrease computational time without significant changes to the numerical solution.

Because AAAs have a complex shape, the finite element method (FEM) was used in computing the stress/strain in the AAA wall, AS, and endograft. The FEM involves breaking the complete, continuous geometry into many smaller geometric elements. In

this study the elements were either triangular (2-D) or tetrahedral (3-D). Further, each element is defined simply by a set of points, or nodes. Together, the elements and nodes make up a mesh. The mesh for each case study of the AAA model was generated with the same software (Patran 2001) used in creating the geometry. Depending on the AAA case being studied, the number of elements ranged from 11,000 to 14,000.

The FEM computations were performed using ABAQUS ver. 6.1-1 (Hibbit, Karlsson and Sorensen, Inc., Pawtucket, RI). After importing the mesh into ABAQUS, the element types were specified. The two-dimensional, shell element type, S3R, was used for both the wall and endograft. S3R elements have 3 nodes with reduced-integration and 5 section points defining its thickness. Shell elements were used for the wall and endograft because their thickness was small in comparison to their diameters. The three-dimensional element, 3D4H, was used for the solid AS contents. 3D4H elements have 4 nodes with hybrid formulation.
Having defined the elements, the elements were given their appropriate material properties as stated above.

Next, the boundary conditions were defined. All nodes located on the ends of the AAA model were constrained from displacing in the longitudinal direction to simulate the experimental setup where the ends of the artificial AAA were fixed. A "no-slip" condition between the wall, AS contents, and endograft was assumed such that the surfaces of differing materials could not slide against each other. A normal peak systolic pressure of 120 mm Hg (16 kPa) was applied to the luminal surface. The solution procedure used a static analysis that accounted for the AAA's nonlinear geometry while gradually applying the pressure load for more accurate results. Shear stresses due to flowing blood were considered negligible because their magnitudes have been shown to be very small in comparison to stress due to the pressure load.[14] The outer surface of the AAA model was assumed to be load free. The effects of residual stresses were not studied nor included into the load conditions. The computational results are displayed in von Mises stress for each case. Von Mises stress accounts for the three principal stresses in a given solid and is a commonly used predictor of material failure.

Results

In the finite element AAA models, the highest stresses occurred at regions in the endograft where the aneurysm wall was furthest away from the endograft (see figs. 4-6). Peak endograft stresses were 112.1, 134.4, and 131.8 kPa for canine models one, two, and three, respectively. The lowest stresses in the endografts occurred at the ends of the aneurysm where the endograft and wall are in close proximity. Minimum endograft stresses were 34.9, 45.1, and 43.7 kPa for canine models one, two, and three, respectively.

The highest stresses in the aneurysm walls occurred at or near the ends of the aneurysm where the wall and endograft converge (figs. 1-3). Peak wall stresses were 52.0, 48.8, and 64.6 kPa for models one, two, and three, respectively. The lowest wall stresses occurred at the bulge of the aneurysm. Minimum wall stresses were 7.1, 2.1, and 3.4 kPa for models one, two, and three, respectively. For the aneurysm wall, stress appears to be inversely proportional to distance from the endograft. (Note that the anterior side is relatively close to the endograft, and the right and left sides are the bulges

of the aneurysms in the canine models). An interesting situation occurred in the third canine model due to the curvature of the endograft. The curvature caused the bulge at the left side to be closer to the endograft and, conversely, caused the right side bulge to be further away (figs. 7-8). Having the endograft in closer proximity, the stresses in the left side bulge were overall higher than in the right side bulge, which was further away from the endograft.

Overall, the stresses were lowest in the aneurysm sac compared to the endograft and wall (figs. 9-11). The highest AS stresses occurred at or near the endograft surfaces. Peak AS stresses were 7, 5, and 5 kPa for models one, two, and three, respectively. The lowest AS stresses occurred at or near the wall surfaces. Minimum AS stresses were 0.7, 0.5, and 0.5 kPa for models one, two, and three, respectively. The greatest reduction in stress in the AS occurred at the wall surface of the bulge of the aneurysm. As with the aneurysm wall, AS stress appears to be inversely proportional to distance from the endograft.

Figures

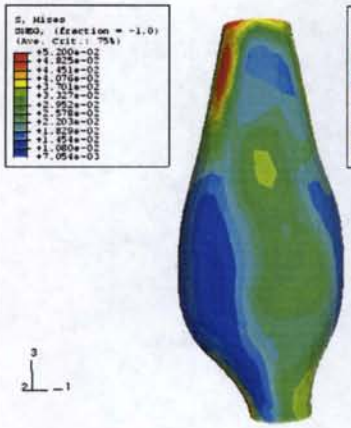

Fig. 1: Dog 1 wall (anterior)

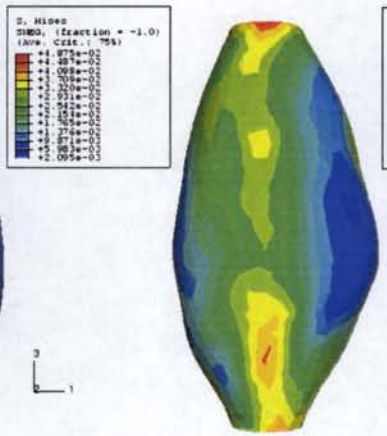

Fig. 2: Dog 2 wall (anterior)

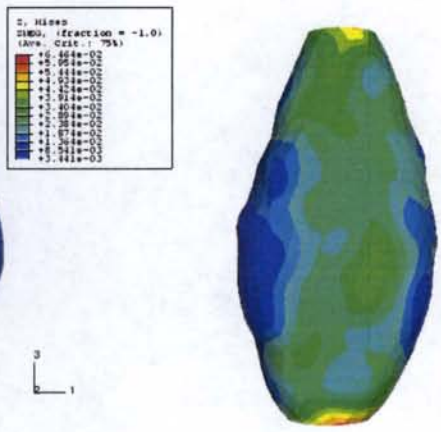

Fig. 3: Dog 3 wall (anterior)

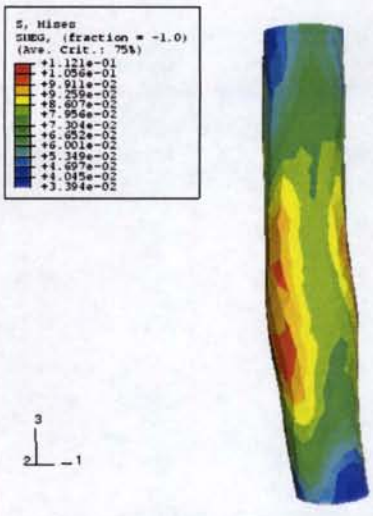

Fig. 4: Dog 1 endograft (anterior)

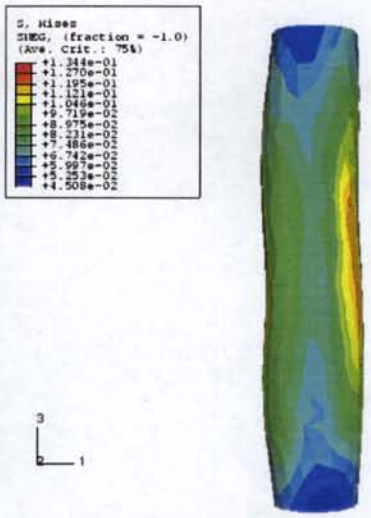

Fig. 5: Dog 2 endograft (anterior)

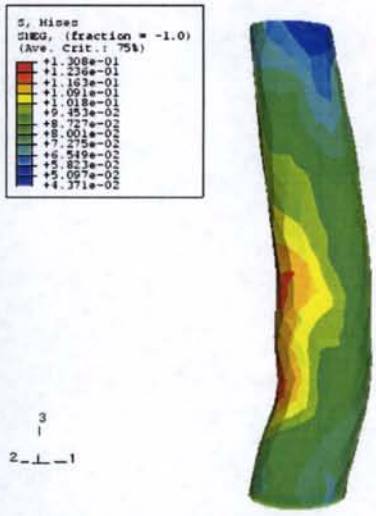

Fig. 6: Dog 3 endograft (anterior)

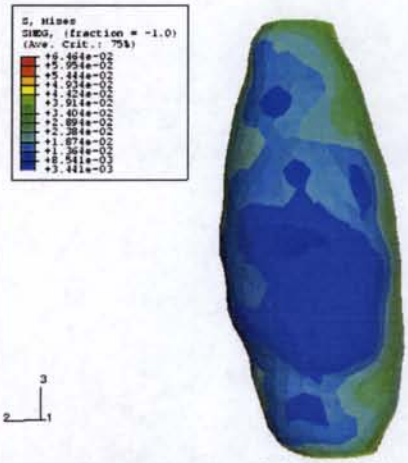

Fig. 7: Dog 3 wall (right side)

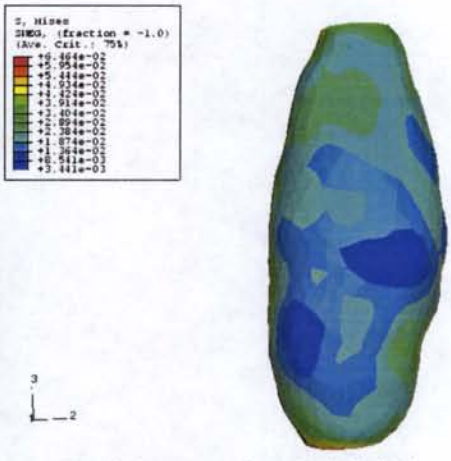

Fig. 8: Dog 3 endograft (left side)

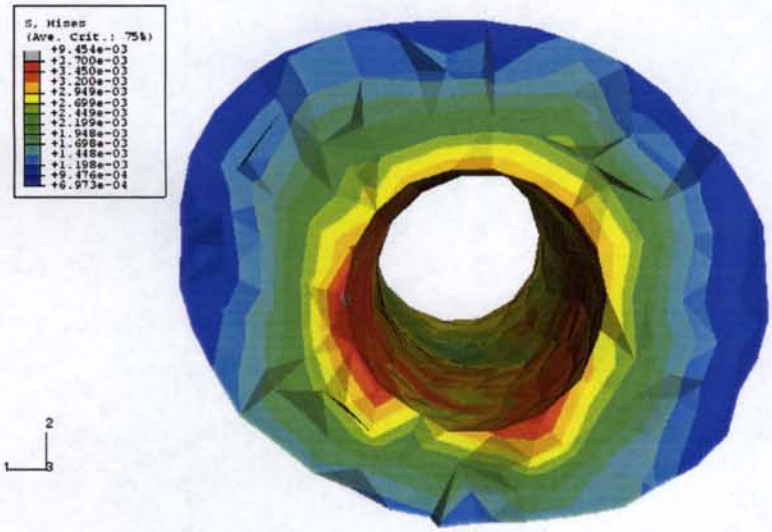

Fig. 9: Dog 1 AS cross-section

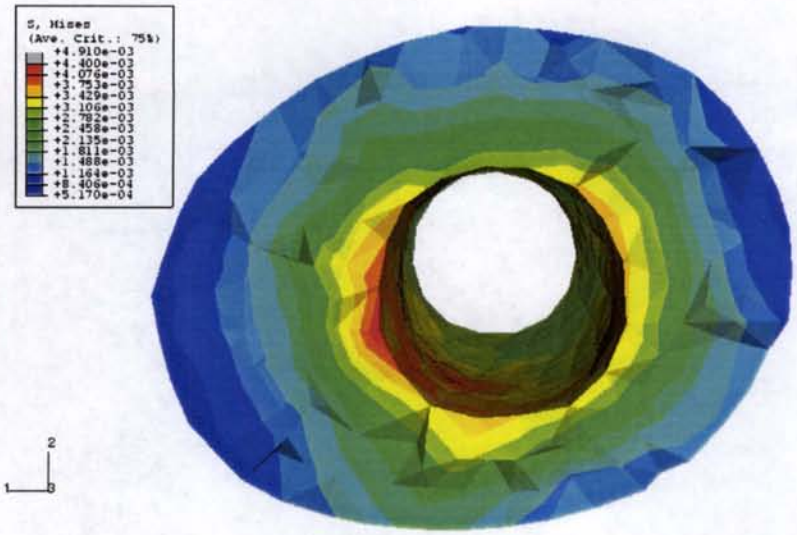

Fig. 10: Dog 2 AS cross-section

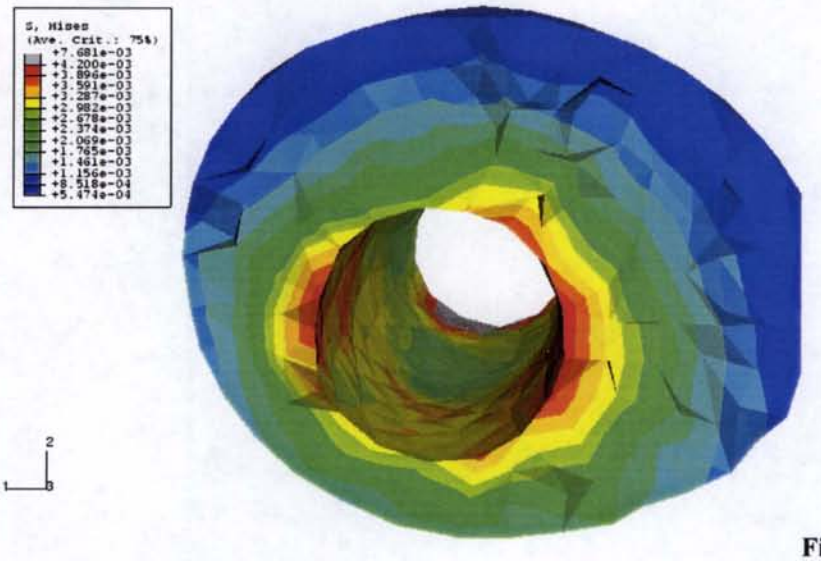

Fig. 11: Dog 3 AS cross-section

Discussion

The results of this study indicate that endotension is a real phenomenon and does not require the presence of endoleak. Supporting evidence for this argument comes from the fact that significant levels of stress were computed for the aneurysm walls in all of the FE models, none of which had endoleak. The magnitude of endotension computed is highly dependent on the material property definitions (i.e. elasticity) of the wall, AS, and endograft. Because the elastic moduli used were rough approximations, this study cannot quantify the magnitude of endotension.

Another finding of this study is that endotension in the aneurysm sac is not uniformly distributed but, instead, is dependent on distance from the endograft. As seen in figures 9-11, stress is highest near the endograft and attenuates with distance from the graft. This result makes sense because the excluded aneurysm is a pressure vessel, which, for simple geometries, have closed-form equations quantifying the decrease in stress as a function of radial distance across the thickness of the vessel membrane.[15] The

attenuation of AS stress in this study relies on the assumption that the AS contents are solid and capable of resisting the deformation of the endograft. The effects of a thrombus that did not completely surround the AS circumferentially were not studied. However, if AS contents are fluid in nature, the AS would not be able to resist the deformation of the endograft. Further, the sac fluid would transmit the load to the wall resulting from graft deformation instead of attenuating the load.

Like the sac, aneurysm wall tension also was found to be dependent on distance from the endograft. The highest stresses occurred near the ends of the aneurysms where the wall and endograft were in close proximity. Conversely, the lowest wall stresses occurred at the bulge of the aneurysm where the wall was farthest away from the endograft. Further support of this argument comes from the overall higher stresses seen at the left side bulge of the third FE model (fig. 8) than the right side bulge (fig. 9) where the curvature of the endograft caused the right side to be farther from the endograft than the left side. The dependence of wall stress on distance from the endograft is a result of the cushioning effect of the solid AS contents. This relationship might be a factor in post-repair neck dilation because it predicts that the aneurysm wall will be subjected to the greatest stress, or endotension, at the ends of the aneurysm sac.

Additionally, the stress distributions of the endografts were studied. Endograft stress had the opposite relationship between stress and distance than that of the aneurysm wall. Instead, the highest endograft stresses occurred where the wall was farthest away from the endograft. Thus, the endograft stresses were highest where the aneurysm bulged, an effect caused by the lack of a stiff material (i.e. the wall) in proximity to the endograft that could bear some of the load. Conversely, the lowest endograft stresses occurred at the ends of the aneurysm sac where the wall was in close proximity to the endograft. We hypothesize that endograft stresses were lowest at the ends due to the proximity of the wall allowing the pressure load to be shared by both the endograft and wall.

As stated previously, this computational study was performed in conjunction with an experimental study[8] on endotension distribution using artificial aneurysms created from canine aortic tissue, which had been excluded with an endograft. (The numerical results of the experimental study are not detailed in this article). The primary goal of performing the computational and experimental studies in conjunction was to allow for the comparison of conclusions. Using strain transducers, the experimental study measured significant levels of pressure in the aneursym sac, regardless of the nature of the AS contents. This finding is further evidence that endotension is a real phenomenon, as the excluded artificial aneurysms had no radiographic signs of endoleak, and supports the same conclusion drawn from the results from the FE analysis. Another finding of both studies was that endotension was not uniformly distributed throughout the aneurysm sac as evident from the variance in experimental pressure measurements at differing AS locations and the AS stress patterns computed by the FE models. Further, both studies determined AS endotension to be higher near the endograft and lower near the wall for an AS composed of blood thrombus in the experimental study and organized intraluminal thrombus in the computational study. Thus, both studies conclude that thrombus reduces pressure transmission to the aneurysm wall. Additionally, the experimental study provided results and conclusions for an aneurysm sac filled with unclotted blood, but this scenario was not studied in the computational study.

Qualitative comparisons between the experimental and computational studies were not performed because the mechanical properties of the canine artificial aneurysms were not available. Thus, the properties used in the computational studies were rough approximations. Further, the FE models used properties of organized intraluminal thrombus for the AS, which are different than the properties of the experimental AS consistencies. Additionally, the stent of the endograft caused enough distortion in the CT images to make it difficult to reconstruct the aneurysm geometry on the computer with great accuracy. Another difficulty in comparing the studies is that pressure and stress are not equivalent mathematical expressions. It was assumed that higher levels of measured pressure or calculated stress indicate higher levels of endotension. However, enough similarity between the two studies exists such that the conclusions of one were able to support or refute the conclusions of the other.

There are a number of limitations of this study due to the assumptions made in the computational models. First, the wall and intraluminal thrombus were assumed to be linearly elastic values but, in reality, have nonlinear stress-strain curves. It is expected that by using linear elastic values that the magnitude of the stress distributions is not accurately predicted but their patterns are accurately predicted. Thus, use of linear elastic values is acceptable for this study because the study does not attempt to make quantitative conclusions. Also, the accuracy of assuming that the AAA wall tissue is homogenous, incompressible, and isotropic has not been evaluated experimentally.[16] Additionally, residual stresses have been shown to potentially result in a significant effect on the wall stresses in nonaneurismal arterial tissue.[17] The presence of residual stresses, which were neglected in this study, in AAA tissue also might affect the stress distribution in AAAs. Another possible source of error could be due to the uniform wall thickness in our FE models. This study did not examine the effects of the varying wall thickness observed in real AAA geometries. Instead of using a static, constant pressure analysis, a dynamic analysis with pulsatile pressure would be more realistic and might give different results for the stress distributions. Also, the appropriateness of using von Mises stress as a descriptor for endotension has not been determined. Another potential source of error was the mesh used for the AS. Near the ends of the FE models, the AS mesh elements were highly skewed, which could have caused numerical inaccuracies at the ends. Additionally, a small number of elements throughout the AS mesh were distorted and could have caused localized stress concentrations.

Future Work. Using the same computational models of this study, more comparable conclusions to the experimental study can be made by studying the effects of varying blood pressure and varying the consistency of the aneurysm sac contents (e.g. unclotted blood, fresh thrombus). Further, using pulsatile pressure loading (instead of static) and experimentally determined constitutive equations for tissue elasticities might provide a sufficiently realistic computational model by which to quantify the magnitude of endotension. An interesting challenge would be to create another combined experimental/computational study that achieved comparable numerical results (i.e. strain/pressure measurements and computed strain or stress). Such an accomplishment would establish an even greater confidence in their results and conclusions. A possible avenue to overcome the difficulty in comparing numerical and experimental models would be to simplify the materials used in the experimental aneurysms. This could be

achieved by using synthetic materials for the aneurysm wall and AS, whose properties could be easily determined.

Acknowledgements

I thank the Department of Surgery of the University of Tennessee Medical Center, Knoxville, and the Division of Computational Science & Engineering of Oak Ridge National Laboratory for funding and equipping my research.

Special thanks go to my research mentor, Kara Kruse, and John Pacanowski, M.D. for their continual guidance and invaluable advice on my research.

Additional thanks go to Scott Stevens, M.D., Mitchell Goldman, M.D., and Michael Freeman, M.D., and the entire staff of the vascular research laboratory at the Univ. of Tennessee Medical Center, Knoxville, for their expertise and consultation from the clinical perspective.

References:

1. Wolf, Y., Hill, B., Rubin, G., Fogarty, T., & Zarins, C. (2000). Rate of change in abdominal aortic aneurysm diameter after endovascular repair. Journal of Vascular Surgery, 32, 108-113.
2. Gilling-Smith, G., Brennan, J., Harris, P., Bakran, A., Gould, D., & McWilliams, R. (1999). Endotension after endovascular aneurysm repair: Definition, classification, and strategies for surveillance and intervention. Journal of Endovascular Surgery, 6, 305-307.
3. Lumsden, A., Allen, R., Chaikof, E., et al. (1995). Delayed rupture of aortic aneurysms following endovascular stent grafting. American Journal of Surgery, 170, 174-178.
4. Malina, M., Ivancev, K., Chuter, T., et al. (1997). Changing aneurismal morphology after endovascular grafting: Relation to leakage or persistent perfusion. Journal of Endovascular Surgery, 4, 23-30.
5. Zarins, C., White, R., & Fogarty, T. (2000). Aneurysm rupture after endovascular repair using the AneuRx stent graft. Journal of Vascular Surgery, 31, 960-970.
6. Makaroun, M., & Deaton, D. (2001). Is proximal aortic neck dilation after endovascular aneurysm exclusion a cause for concern? Journal of Vascular Surgery, 33, s39-45.
7. Gould, D., Edwards, R., McWilliams, R., et al. (2000). Graft distortion after endovascular repair of abdominal aortic aneurysm: Association with sac morphology and mid-term complications. Cardiovascular and Interventional Radiology, 23, 358-363.
8. Pacanowski, J., Stevens, S., Freeman, M., et al. (in print). Endotension distribution and the role of thrombus following endovascular abdominal aortic aneurysm (EAAA) exclusion. Journal of Endovascular Therapy.
9. Smith, D., Sacks, M., Vorp, D., & Thornton, M. (2000). Surface geometric analysis of anatomical structures using biquintic finite element interpolation. Annals of Biomedical Engineering, 28, 598-611.
10. Raghavan, M., Webster, M., & Vorp, D. (1996). *Ex vivo* biomechanical behavior of abdominal aortic aneurysm: Assessment using a new mathematical model. Annals of Biomedical Engineering, 24, 573-582.
11. Vorp, D., Raghavan, M., Muluk, S., Makaroun, M., Steed, D., Shapiro R., et al. (1996). Wall strength and stiffness of aneurysmal and nonaneurysmal abdominal aorta. Annals New York Academy of Sciences, 800, 274-276.
12. Inzoli, F., Boschetti, F., Zappa, M., Longo, T., & Fumero, R. (1993). Biomechanical factors in abdominal aortic aneurysm rupture. European Journal of Vascular Surgery, 7, 667-674.
13. Vorp, D., Raghavan, M., Borovetz, H., Greisler H., & Webster, M. (1995). Modeling the transmural stress distribution during healing of bioresorbable vascular prostheses. Annals of Biomedical Engineering, 23, 178-188.
14. Bluestein, D., Niu, L., Schoephoerster, R., & Dewanjee, M. (1996). Steady flow in an aneurysm model: Correlation between fluid dynamics and blood platelet deposition. Journal of Biomechanical Engineering, 118, 280-286.

15. Riley, W., Sturges, L., & Morris, D. (1998). Mechanics of Materials. 5th ed. Wiley, New York.
16. Raghavan, M., & Vorp, D. (2000). Toward a biomechanical tool to evaluate rupture potential of abdominal aortic aneurysm: Identification of a finite strain constitutive model and evaluation of its applicability. Journal of Biomechanics, 33, 475-482.
17. Delfino, A., Stergiopulos, N., Moore, J., & Meister, J. (1997). Residual strain effects on the stress field in a thick walled FE model of the human carotid bifurcation. Journal of Biomechanics, 30, 777-786.